UNIVERSITY OF GRONINGEN

BACHELOR THESIS

Did Leo I collide with the Magellanic Clouds?

Author:
Ewoud WEMPE

Supervisor:
Prof. Amina HELMI

A thesis submitted in fulfillment of the requirements for the degree of Bachelor Astronomy

in the

Kapteyn Astronomical Institute
Faculty of Science and Engineering

July 10, 2018

Abstract

Ewoud WEMPE

Did Leo I collide with the Magellanic Clouds?

Because of its high velocity at its large distance, Leo I could be unbound. Although it is rare to have unbound satellites at Leo I's distance, a possible explanation for this would be that it had an encounter with the Magellanic Clouds. In this thesis, this possibility is explored.

For a combination of possible Galactic potentials and Magellanic Clouds profiles, the probability that the Magellanic Clouds had an encounter with Leo I was evaluated. Few such orbits were found: in the model where an encounter was most likely (this model combines heavy Magellanic Clouds with a light Milky Way), only 4.36% of the realizations satisfied the strong encounter criterion. When only considering realizations where the LMC and Leo I are not currently at their minimum distance, the probability becomes 9.98%.

Contents

Chapter 1

Introduction

One of the big open questions in astrophysics is how much dark matter there is in galaxies, and in particular the Milky Way. Finding the mass of the Milky Way is not easy, especially at large distances, but one constraint often used comes from the dwarf galaxy Leo I, the most distant satellite of the Milky Way.

1.1 The Leo I dwarf galaxy

The kinematics of the Leo I dwarf galaxy are very interesting. It is the most energetic of the large satellite galaxies that orbit the Milky Way, with a line of sight velocity of $v_{\mathrm{LOS}} = (282.5 \pm 0.1)\,\mathrm{km/s}$ and a distance of $d = (254 \pm 15)\,\mathrm{kpc}$ (McConnachie, 2012). Given the various estimates of the Milky Way mass, this high velocity implies that Leo I could be unbound[1]. But Boylan-Kolchin et al. (2013) showed that it is vanishingly rare to have unbound satellites at distances of Leo I in ΛCDM simulations. That is why Leo I being bound can be used as a constraint on the mass of the Galaxy. In particular, for the Gaia proper motions this gives a lower limit of $M_{\mathrm{MW}}(r_{\mathrm{LeoI}}) = 9.1 \times 10^{11}{}^{+6.2}_{-2.6}\,\mathrm{M}_{\odot}$, under the assumption of a NFW profile with $r_s = 18.6\,\mathrm{kpc}$ (Gaia Collaboration et al., 2018). Sales et al. (2007) showed that in their N-body simulations, the cases where there was a satellite with such a high energy, it was the result of a three-body encounter with a heavier satellite. They argued that maybe Leo I also had such an encounter. That gives a problem: if the large energy of Leo I is due to a three-body encounter, it might not be bound, and the constraint on the mass of the Milky Way is no longer applicable. So that raises the question: could Leo I have had an encounter with another satellite galaxy in the past?

1.2 The Magellanic Clouds

Because of their high mass, an attractive scenario is an encounter with the Magellanic Clouds. A main motivation for looking at the Magellanic Clouds was that they had similar pericenter times in the traditional orbital models (Murai and Fujimoto, 1980; Gardiner and Noguchi, 1996; Gardiner, Sawa, and Fujimoto, 1994).

1.2.1 Orbital history

The details of the orbits of the Magellanic Clouds have been under debate in the last decades. Traditionally, it was thought that the Clouds had several pericenters around the Galaxy, the most recent occurring ∼1.5 Gyr ago (Murai and Fujimoto, 1980). But more recent accurate proper motion measurements that were made by

[1] A satellite is bound if the velocity is smaller than the nominal escape velocity (Sales et al., 2007), or equivalently, if the sum of its kinetic and potential energy is negative ($T + \Phi < 0$).

the Hubble Space Telescope, revealed that the LMC had a much larger tangential velocity than previously thought (Kallivayalil et al., 2006). Because of this, it has become a possibility that the Clouds are currently on first infall, and are currently at pericenter (Besla et al., 2007). That is attractive, because it explains why the Magellanic Clouds are outliers in appearance (they look irregular compared to the other satellite galaxies and are star forming) and kinematics (they move faster). But this scenario does cause difficulties when trying to model the formation of the Magellanic Stream. It can no longer be explained by the traditional tidal and ram pressure stripping models, which is why others also propose scenarios in which the Clouds are now at second pericenter (Bekki, 2011; Zhang et al., 2012).

1.2.2 Mass

Next to the proper motions, the LMC mass is also an important parameter when calculating the orbits. When integrating orbits directly, a heavy Large Magellanic Cloud works best to support a first-infall scenario. Due to the small extent of the circular velocity profile, determining the mass by fitting the rotation curve still leaves much uncertainty. For example, in Buckley et al. (2015) the rotation curves were fitted, giving possible virial masses ranging from $5.0 \times 10^{10}\,\mathrm{M}_\odot$ to $1.9 \times 10^{11}\,\mathrm{M}_\odot$. Another argument for the Cloud masses follows from assuming a baryonic mass and a baryon fraction. By requiring the baryon fraction $M_{\mathrm{bar}}/M_{\mathrm{tot}}$ to be equal to cosmological expectations, masses ranging from $6 \times 10^{10}\,\mathrm{M}_\odot$ to $25 \times 10^{10}\,\mathrm{M}_\odot$ are found (Besla, 2015). This mass range was found by using the relations from Moster, Naab, and White (2013), in which the authors relate stellar and halo masses by fitting to dark matter simulations, at different infall redshifts. These masses therefore refer to the virial mass at infall. Currently, the mass that is still bound is significantly smaller, because satellites lose mass during their infall. Ideally one would use a model that accounts for this mass loss, but for simplicity in this analysis I used a constant mass. The time of infall is roughly the time that Leo I could have had an interaction with the Clouds, so infall masses are relevant, but I will also explore lower masses, that are more consistent with the current bound mass.

1.2.3 The LMC-SMC pair

Another piece of evidence supporting a heavy LMC-SMC pair in combination in a first infall scenario is the large relative velocity of the Clouds. The Magellanic Clouds have been interacting with each other for at least a few Gyr, but maybe longer. The most obvious evidence for their present day interaction is the bridge of material connecting the two Magellanic Clouds. Likely, this is the formed in tidal interactions between the Clouds during their close passage (Gardiner and Noguchi, 1996). More evidence is for example in the star formation history (Weisz et al., 2013). The star formation rate started increasing for both the LMC and the SMC 4 Gyr ago, so it is reasonable to assume they at least have been interacting since then. But to keep the Clouds bound for such a long time with such high relative velocities, relatively high masses are necessary (Besla, 2015).

1.3 This thesis

In this thesis, I will model the orbits of Leo I and the Magellanic Clouds, and explore what the probability for an encounter is. In Chapter 2, I will explain the model. First, I discuss how initial conditions were chosen (Section 2.1), the various Galactic

and satellite potentials used (Section 2.2), and dynamical friction (Section 2.3). Next, in Chapter 3, the results are shown, first exploring the different models (Section 3.1) and then looking at the Monte Carlo simulations that take into account the observational uncertainties (Section 3.2). In Chapter 4 the main conclusions are summarized, and shortcomings and validity of the analysis are discussed.

Chapter 2

Integrating the orbits

To solve the equations of motion, a numerical integrator is used, because the relevant equations are generally not analytically solvable. Often, orbits are integrated using a symplectic integrator, such as the Leapfrog integrator. If the problem has the right symmetries, this is beneficial, because for the same computational effort, numerical errors in the energy or angular momentum do not grow over time as much as they would in a non-symplectic integrator (Binney and Tremaine, 2008). Another advantage is that they are time-reversible, which means that integrating forward, and then taking the result as new initial conditions and integrating backwards, gives the exact initial condition of the starting point.

Instead, I used a Runga-kutta 4 integrator, because due to dynamical friction, energy and angular momentum are not conserved anyway. I used a step size of 0.1 Myr: this resulted in reasonably small errors. In particular, when integrating in a static Galactic potential without interactions and dynamical friction, the relative energy and L_z errors (i.e. $\frac{E(t=-10\,\mathrm{Gyr})-E(t=0)}{E(t=0)}$ and $\frac{L_z(t=-10\,\mathrm{Gyr})-L_z(t=0)}{L_z(t=0)}$) were of the order $\lesssim 10^{-12}$. The resulting positions and velocities were saved every $\sim 10\,\mathrm{Myr}$. Such low errors and frequent output might not be necessary, but it rules out numerical errors as the cause for any phenomena that are explored.

2.1 Initial conditions

The present-day sky positions and proper motions of all satellites were taken from Gaia Collaboration et al. (2018, their Table C.2). Distances and radial velocities were taken from McConnachie (2012). For generating a sample of initial conditions, the observed quantities (distance d, proper motions μ_α, μ_δ and line-of-sight velocity v_{LOS}) were convolved with their uncertainties. Gaussian errors were assumed, and for the proper motions, a covariance matrix was used to take into account the error correlation. Subsequently, to these generated μ_α and μ_δ, an extra systematic uncertainty of $35\,\mu\mathrm{as\,yr}^{-1}$ was added in both directions. This systematic uncertainty was generated separately for each satellite. So in total, $(\mu_\alpha, \mu_\delta)_{\text{Monte Carlo}} = (\mu_\alpha, \mu_\delta)_{\text{mean}} + \mathcal{N}((0,0), \mathbf{\Sigma}_{\text{stat}}) + \mathcal{N}((0,0), (0.035\,\mathrm{mas\,yr}^{-1})^2)$.

The systematic errors are local variations, that arise because of the non-uniform sky scanning pattern. This effect is actually visible in the proper motion maps for the Magellanic Clouds, where one can see a banding pattern (Gaia Collaboration et al., 2018). Because the Magellanic Clouds are quite extended, the proper motion measurements might be slightly more robust, but I stayed conservative and kept it at the $0.035\,\mathrm{mas\,yr}^{-1}$ the authors recommend.

α and δ were not convolved with any errors, because of the negligible uncertainty compared to the rest, even when considering the difference between the possible dynamical centers for the LMC.

Next, a transformation was made to a Galactocentric reference frame, for which the `astropy` module (Astropy developers, 2018) was used. For this, a Solar Galactocentric distance of 8.3 kpc (Gillessen et al., 2009) was assumed, with a $v_c(R_0) = 235\,\mathrm{km\,s^{-1}}$, and a peculiar velocity of $(U, V, W)_{\mathrm{solar}} = (11.1, 12.24, 7.25)\,\mathrm{km\,s^{-1}}$ (Schönrich, Binney, and Dehnen, 2010). For simplicity, uncertainties in these parameters were not convolved.

2.2 Galactic and satellite potentials

To model the Milky Way potential as accurately as possible, a combination of several potentials was used, to model the disk, bulge and halo separately. For the purposes of this analysis however, the most important component is the halo. To describe the dark matter halo, a Navarro-Frenk-White (NFW) profile was used (Binney and Tremaine, 2008; Navarro, Frenk, and White, 1996). Another simple model is a logarithmic halo (Binney and Tremaine, 2008; Helmi et al., 2017), but there is a wide variety of possible halo profiles (Gaia Collaboration et al., 2018).

The NFW potential is particularly useful, because it provides a good fit for ΛCDM dark matter halos from ΛCDM simulations. It has two free parameters, the virial mass, and the concentration. The virial mass is sometimes defined such that the total density inside the virial radius is $\rho_{\mathrm{vir}} = \Delta_{\mathrm{vir}}\Omega_m\rho_c$, where Δ_{vir} is the virial overdensity (which depends on the redshift and the cosmology used), Ω_m is the matter density parameter and ρ_c is the critical density. Instead, I use the definition, where M_{200} is defined such that $\rho_{200} = 200\rho_c$. For ρ_c, I used the value calculated by `astropy`, using parameters from Planck Collaboration et al. (2016). For simulated halos, the concentration parameter c_{200} was found to be very correlated to M_{200} (Dutton and Macciò, 2014). The mass of an NFW halo diverges, so sometimes a cutoff is implemented, but I did not do that for any of the models used here.

Hernquist Bulge	$\Phi(r) = -\frac{GM_{\mathrm{bulge}}}{r+c_b}$
Miyamoto-Nagai disk	$\Phi(R,z) = -\frac{GM_{\mathrm{disk}}}{\sqrt{R^2+(a_d+\sqrt{z^2+b_d^2})^2}}$
NFW halo	$\Phi(r) = -\frac{GM_{200}}{g(c_{200})r}\ln\left(1+\frac{r}{r_s}\right)$
Logarithmic halo	$\Phi(r) = v_h^2\ln\left(1+\frac{r^2}{a_h^2}\right)$
Plummer potential	$\Phi(r) = -\frac{GM}{\sqrt{r^2+a_{\mathrm{plum}}^2}}$

TABLE 2.1: Some of the potentials that were used.

For the orbital integrations, I considered 3 Galactic potential models, their circular velocity profiles are plotted in Figure 2.1:

- Model 1 is from Price-Whelan (2017), using a disc model from Bovy (2015). It has a spherical Hernquist Bulge ($M_b = 5\times10^9\,\mathrm{M_\odot}$, $c_b = 1\,\mathrm{kpc}$), a spherical nucleus (Hernquist, $M_n = 1.71\times10^9\,\mathrm{M_\odot}$, $c_n = 0.07\,\mathrm{kpc}$), a Miyamoto-Nagai disk ($M_d = 6.8\times10^{10}\,\mathrm{M_\odot}$, $a_d = 3\,\mathrm{kpc}$, $b_d = 0.28\,\mathrm{kpc}$), and an NFW halo ($M_{200} = 9.3\times10^{11}\,\mathrm{M_\odot}$, $c_{200} = 13.2$).
- Model 2 has a Hernquist Bulge ($M_b = 3.4\times10^{10}\,\mathrm{M_\odot}$, $c_b = 0.7\,\mathrm{kpc}$), Miyamoto-Nagai disk ($M_d = 1\times10^{11}\,\mathrm{M_\odot}$, $a_d = 6.5\,\mathrm{kpc}$, $b_d = 0.26\,\mathrm{kpc}$) and an NFW halo ($M_{200} = 1.5\times10^{12}\,\mathrm{M_\odot}$, $c_{200} = 8.0$). This bulge and disk model was taken from

Re Fiorentin et al. (2005), and I replaced the log-halo with an NFW halo. The NFW concentration was calculated using the mass-concentration correlation from Dutton and Macciò (2014): $\log_{10}(c) = 0.905 - 0.101 \log_{10}(M_{200}/[10^{12} h^{-1} \mathrm{M}_\odot])$.

- Model 3 has the same bulge and disk model as Model 2, but a heavier NFW halo ($M_{200} = 2.0 \times 10^{12}\,\mathrm{M}_\odot$, $c_{200} = 7.8$). The NFW concentration was calculated in the same way.

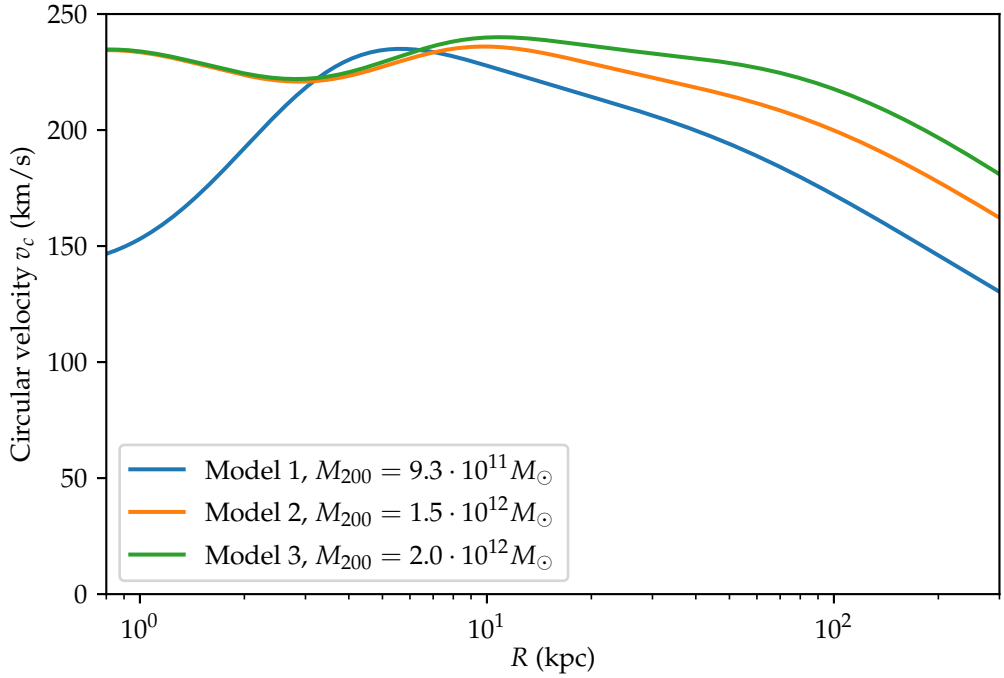

FIGURE 2.1: Circular velocity profiles for the different Milky Way models considered.

The LMC and Leo I were modelled as Plummer spheres, as was done in Sohn et al. (2013). Because these masses are not well known, I considered LMC masses ranging from $2.5 \times 10^{10}\,\mathrm{M}_\odot$ to $2 \times 10^{11}\,\mathrm{M}_\odot$ (see Section 1.2.2). To get reasonable dimensions of the LMC, the Plummer scale radii were obtained by using a cosmological concentration-mass correlation (Correa et al., 2015). To get reasonably similar velocity profiles, I set $a_{\mathrm{plum}} = 2r_{s,\mathrm{NFW}}$. This choice is somewhat arbitrary, but for example for a $1 \times 10^{11}\,\mathrm{M}_\odot$ LMC, this results in an equal enclosed mass at 12.6 kpc. This is roughly the tidal radius at present for the LMC: $r_t = 11$ kpc using Equation (10) from Zentner and Bullock (2003) (and in fact, for the heavier LMC models, the LMC is currently at pericenter). The total mass is the same as the NFW M_{200}. The difference between the circular velocity profiles is shown in Figure 2.2.

2.3 Dynamical friction

Simply integrating the orbits in the gravitational potential of the Milky Way does however not give realistic results, because there would be no orbital decay, which is important for massive galaxies like the LMC. When a subject body moves through some extended host, the particles from the host will interact with the subject body.

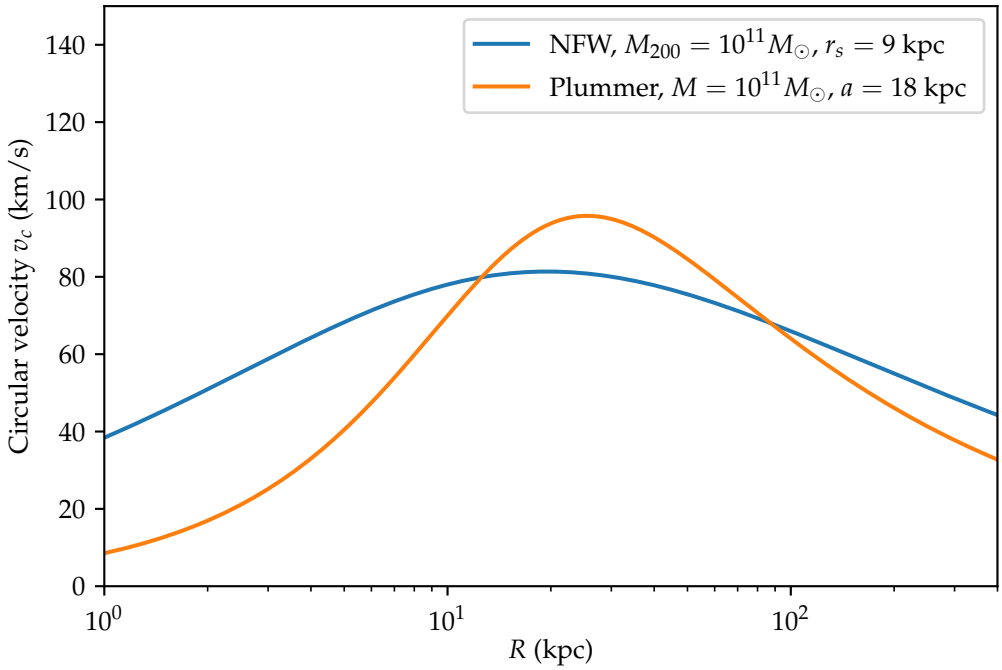

FIGURE 2.2: The difference between the Plummer and NFW circular velocity profiles for a satellite resembling in mass the LMC. The choice of $a_{\rm plum} = 2r_s$ results roughly equal enclosed masses at the LMC's estimated tidal radius by Zentner and Bullock (2003, their Equation (10)).

But in these interactions, the (light) particles from the host can accelerate and gain kinetic energy. That energy must then come from the subject body, so that will be slowed down: there is a friction force. For small masses, this force is often negligible, as dynamical friction is strongest when the host and satellite masses are similar. An expression for the acceleration due to this force was found in Chandrasekhar (1943). A complete derivation is in Binney and Tremaine (2008), but it comes down to integrating over all possible encounters that the host particles can have. The equation reads:

$$\frac{\mathrm{d}\mathbf{v}}{\mathrm{d}t} = -\frac{4\pi \ln\Lambda G^2 M_{\rm sat}\rho_{\rm host}}{v_{\rm orb}^2}\left(\mathrm{erf}(X) - 2Xe^{-X^2}\right)\frac{\mathbf{v}_{\rm orb}}{v_{\rm orb}}, \tag{2.1}$$

where $X = v_{\rm orb}/\sqrt{2\sigma^2}$, where σ is the one-dimensional velocity dispersion. Zentner and Bullock (2003, their Equation (6)) determined an approximation for the velocity dispersion of an NFW profile.

There has been some discussion about the value that should be assumed for the Coulomb logarithm, $\ln\Lambda$. It is defined as $\ln\Lambda = \ln\left(\frac{b_{\rm max}}{b_{\rm min}}\right)$, where $b_{\rm max}$ and $b_{\rm min}$ are the maximal and minimal impact parameters where a collission can be considered efficient. Since the approximation of a constant $\ln\Lambda$ overestimates the circularization, Hashimoto, Funato, and Makino (2003) and Zentner and Bullock (2003) instead set $b_{\rm max} = r(t)$ equal to the Galactocentric distance, and calculate $b_{\rm min}$ by the prescription of White (1976). The recipe of Hashimoto, Funato, and Makino (2003) is followed here and briefly explained in what follows. In White (1976), the following

$M_{\rm LMC}$ (10^{10} $M_\odot$)	$a_{\rm LMC}$ (kpc)	$M_{\rm LeoI}$ (10^8 $M_\odot$)	$a_{\rm LeoI}$ (kpc)
2.5	10.3	0.65	0.986
5	13.6	1.3	1.29
10	18	2.6	1.68
15	21.3	3.9	1.97
20	24	5.2	2.21

TABLE 2.2: The different satellite models explored. In hindsight, there is no need to vary the Leo I mass. However, it would not have made any difference, since dynamical friction is still negligible for Leo I, and Leo I also can not significantly perturb the Magellanic Clouds, given the low mass.

integral is found for the Coulomb logarithm:

$$\ln\Lambda = \frac{1}{M_{\rm sat}^2}\int_0^{b_{\rm max}} D^3\left(\int_D^\infty \frac{M(r)\,{\rm d}r}{r^2(r^2-D^2)^{1/2}}\right)^2 {\rm d}D \tag{2.2}$$

This comes from integrating the forces of particles on hyperbolic paths to find $\Delta v_\parallel$, and subsequently following the (long) mathematical treatment of Chandrasekhar. For Plummer subhalos, this integral can be calculated analytically.

$$\ln\Lambda(x_{\rm sat} = \frac{r}{a_{\rm plum}}) = \frac{(x_{\rm sat}^2+1)^3}{x_{\rm sat}^6} I(x_{\rm sat}) \tag{2.3}$$

$$I(x_{\rm sat} = \frac{r}{a_{\rm plum}}) = \int_0^{x_{\rm sat}} x_b^3\left(\int_{x_b}^\infty \frac{x^3/(x^2+1)^{3/2}}{x^2\sqrt{x^2-x_b^2}}\,{\rm d}x\right)^2 {\rm d}x_b \tag{2.4}$$

$$= \frac{1}{2}\left(\frac{1}{1+x_{\rm sat}^2} - 1 + \ln\left(1+x_{\rm sat}^2\right)\right) \tag{2.5}$$

At $r(t) \gtrsim 5a$, this is well approximated by $\ln\Lambda = \ln\frac{r(t)}{1.6a}$. Hashimoto, Funato, and Makino (2003) calibrated the cutoff radius to N-body simulations, and they found that $\ln\Lambda = \ln\frac{r(t)}{1.4a}$ gave a better match to their simulations. Possibly, they argue, this is because of some the straight-line orbit approximation that Chandrasekhar's formula assumes, while in reality the orbits are more elliptical.

Chapter 3

Results

3.1 Orbits without uncertainties

First, the orbits were integrated backwards in time without any dynamical friction, as point-masses only experiencing the host potential. For the nominal values of the parameters, without errors, the orbits are plotted in the top left panel of Figure 3.1.

Especially in the more massive Galactic potentials, the LMC makes multiple pericentric passages, reminiscent of the traditional models for the Magellanic Clouds orbits. This is not very realistic, because as explained in Section 1.2.1, a first infall scenario is more likely. The reason for this is that no dynamical friction has been included.

After adding dynamical friction, as described in Section 2.3, the orbit of the LMC changes significantly. Firstly, for the LMC model with a traditional mass of $M = 5 \times 10^{10}\,\mathrm{M}_\odot$ the orbits were plotted in the top right of Figure 3.1, and secondly for a heavier LMC of $M = 1.5 \times 10^{11}\,\mathrm{M}_\odot$, as shown in the bottom left panel of Figure 3.1 (the other parameters for this model are listed in Table 2.2). Here one can see the effect of dynamical friction. When integrating back, it results in much more energetic orbits in the past. Still, the LMC stays bound to the Milky Way in all models, and similar to the orbits without dynamical friction, multiple past LMC pericenters exist. After adding dynamical friction the orbital period is much longer. The period is not always as large as the Hubble time, which is what one could expect in a first infall scenario. But of course this model does not work when integrating back too far. One reason for that is that I assumed static potentials for all bodies, while in reality the Milky Way grows significantly over that timespan. The orbit of Leo I does not change visibly when adding dynamical friction, which makes sense considering its relatively small mass. After adding an interaction term so that the satellites attract each other, the Leo I orbit changes slightly (see the bottom right panel of Figure 3.1). The relative distances between Leo I and the LMC are shown in Figure 3.2.

3.2 Monte Carlo realizations

So far, only the orbits for the nominal values (i.e. without considering any errors) of the parameters were calculated. To draw any conclusions, it is necessary to see how the orbits behave when considering different initial conditions. That is why, for 10000 different sets of observables, obtained as explained in Section 2.1, the orbits were calculated, considering inter-satellite interactions and dynamical friction. For the Milky Way, I considered the 3 models described in Section 2.2. I considered different LMC masses, while keeping its mass-ratio to Leo I the same (see Table 2.2).

To get an idea of how likely an encounter between Leo I and the Magellanic Clouds was, I plotted the distributions of minimum distances between the satellites

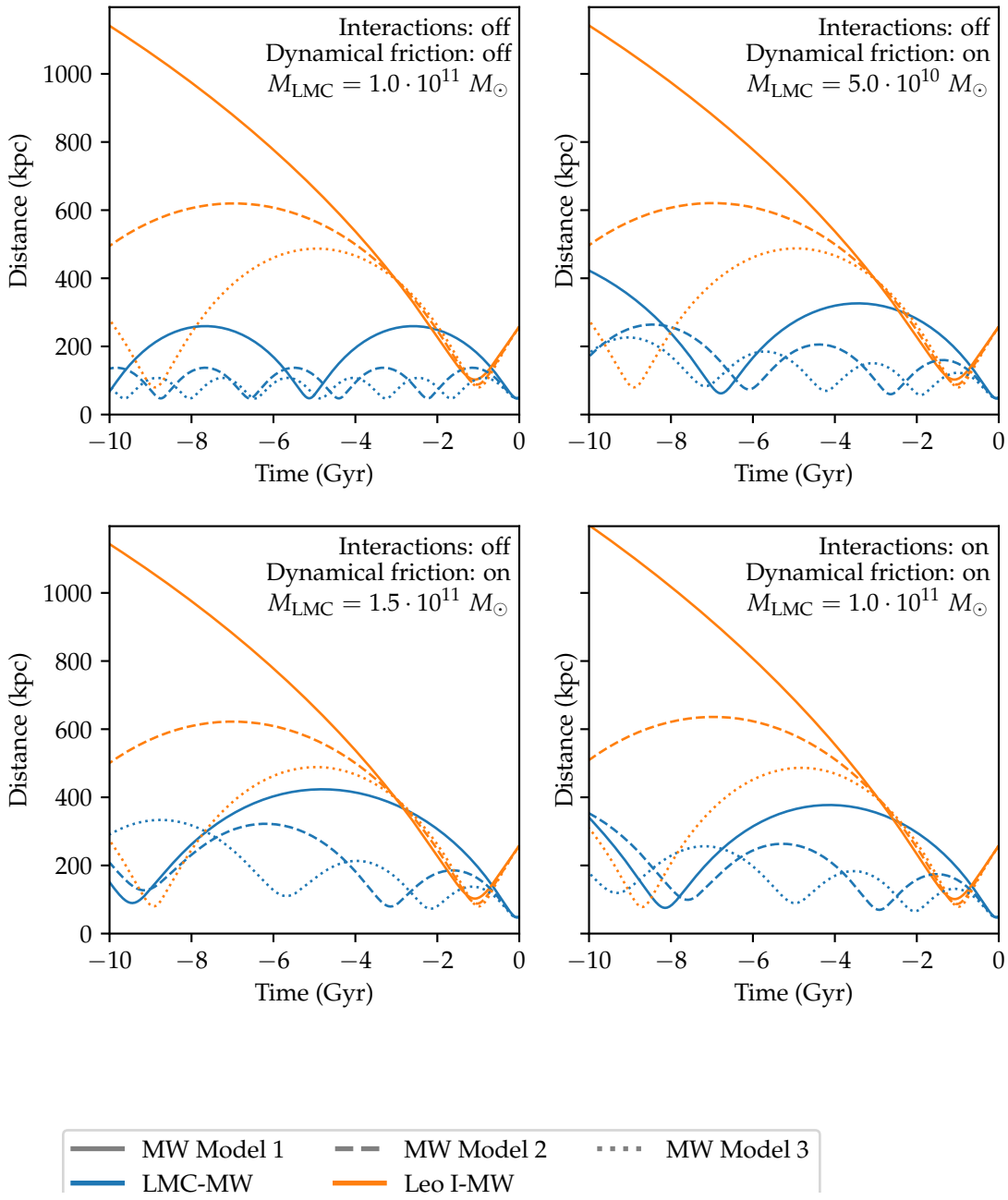

FIGURE 3.1: Galactocentric distances for the satellites in various models, considering various Galactic Potentials.

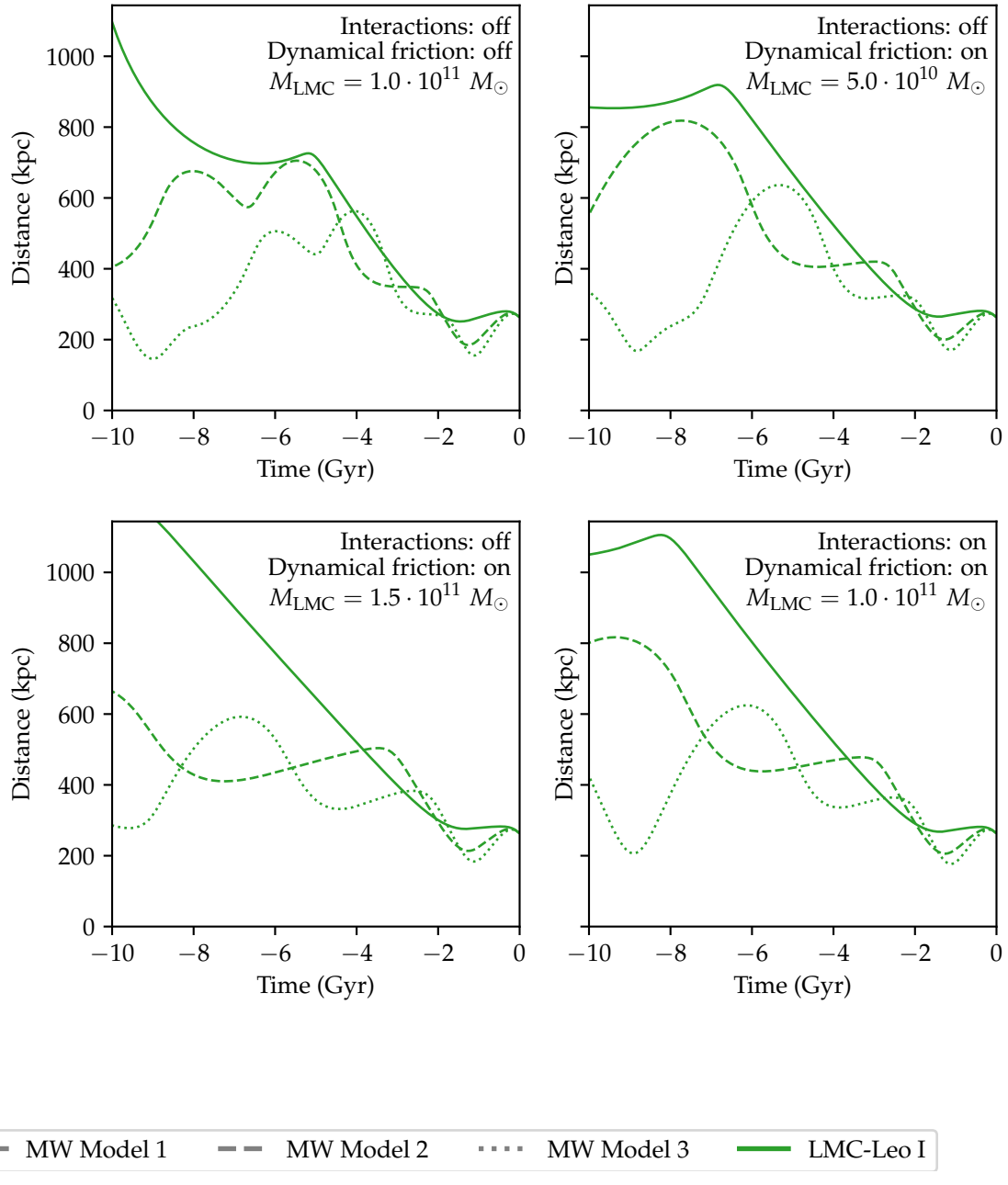

FIGURE 3.2: Relative distances between the LMC and Leo I for the same models as in Figure 3.1.

and the Milky Way in Figure 3.3. Immediately it can be noticed that the probabilities that Leo I and the LMC come close are not very high.

Although the LMC pericenter distribution is fairly narrow, the distribution for Leo I looks very broad. However, it is reasonably consistent with the values provided in Gaia Collaboration et al. (2018). When calculating the pericenter median, 16% and 84% percentile values for the pericenters, the values are very similar: I find $123.3^{+61.4}_{-72.0}$ kpc, $107.6^{+66.9}_{-63.8}$ kpc and $98.4^{+68.6}_{-58.5}$ kpc for Model 1, 2 and 3. The values and the spread are slightly higher than the results in the Gaia paper ($89.5^{+55.9}_{-47.5}$ kpc, $112.6^{+58.4}_{-60.6}$ kpc, $86.9^{+59.2}_{-44.4}$ kpc, for their different models). The different values reflect that different Galactic potentials were used. The slightly higher spread might be because for Leo I, I used the distance uncertainty indicated in McConnachie (2012), which is 5.9%, while the authors of the Gaia paper assumed an error of 2.3%.

3.2.1 Diverging Leo I-LMC realizations

Especially in the light Milky Way models, there is a large amount of realizations where Leo I and the LMC do not come close at any point, while in most realizations, they come closest around 1.5 Gyr ago. This is shown in Figure 3.4, where the times of minimum Leo I-LMC distance are plotted. One can see a significant spike at $t = 0$. But in these realizations, there is certainly not any encounter going on: their physical separation is (264 ± 15) kpc. Another effect on the Leo I - LMC minimum distance distribution is that it becomes bimodal when including these realizations. For clarity of the plots (especially the plots showing the encounter criteria), I therefore only kept the realizations where the time at minimum LMC-Leo I distance is $t_{\mathrm{min}} < -0.5\,\mathrm{Gyr}$. In these plots N denotes the number of realizations where this indeed was the case.

3.2.2 Quantifying encounters

One indicator of whether an interaction has occurred is the force ratio of the Milky Way and the LMC that Leo I experiences, $F_{\mathrm{MW}}/F_{\mathrm{LMC}}$, at the time of minimum LMC - Leo I distance. If this ratio is low, one would expect a large influence of the LMC. In Figure 3.5, the force ratios are shown, but most are around $F_{\mathrm{MW}}/F_{\mathrm{LMC}} = 50$ at the closest approach. Only in a few cases, a force ratio which is less than 1 is obtained. The actual numbers of realizations are listed in Table 3.1. Less than $\sim$3 % of realizations have such a force ratio, while of the realizations with $t_{\mathrm{min}} < -0.5\,\mathrm{Gyr}$ this is less than 6 %

Another indicator to see if an interaction occurred is to use the strong encounter criterion. Sparke and Gallagher (2007) state that there is a strong encounter if, at their closest approach the change in potential energy Φ, is larger than the relative starting kinetic energy before the encounter. Let $t = t_{\mathrm{min}}$ be the time at closest approach, and let $t = t_0$ be the starting time. Let T denote the kinetic energy and Φ the potential energy. Then, the criterion can be written as:

$$\text{Strong encounter} \Leftrightarrow |\Delta\Phi| = \Phi(t = t_0) - \Phi(t = t_{\mathrm{min}}) > T(t = t_0) \tag{3.1}$$

This time t_0, the time before the encounter, is not very well defined in practice. It would be most convenient to have a definition that only depends on the energies at t_{min}. For this, I made the approximation that in the LMC rest frame, energy is

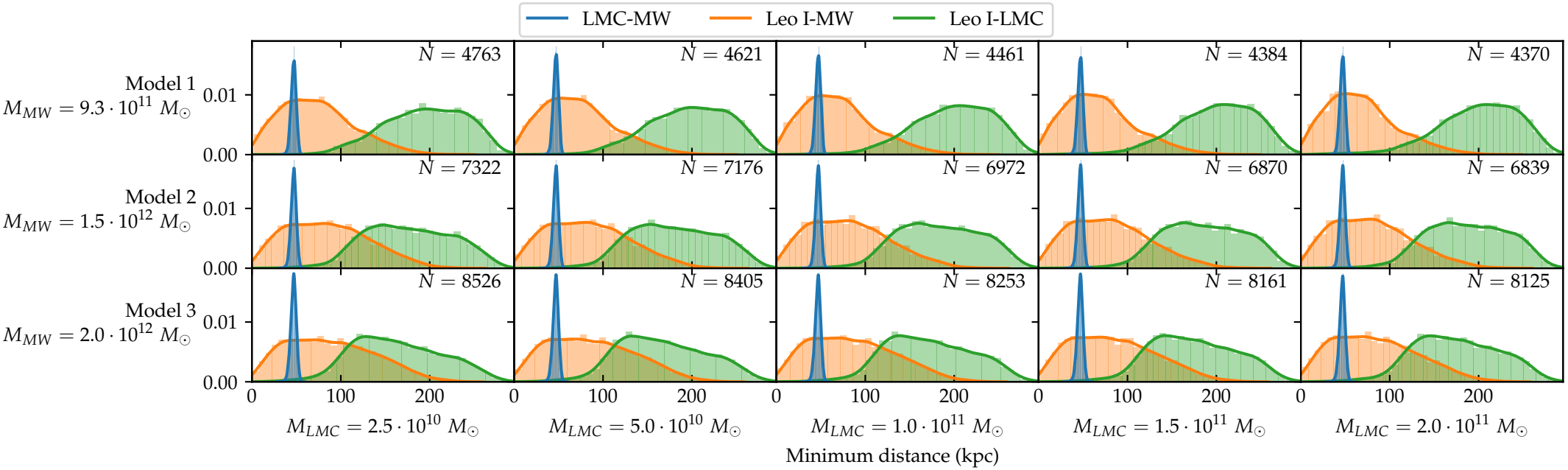

FIGURE 3.3: Minimum distance probability distributions, showing how close the Milky Way and the satellites approach each other. N indicates the number of realizations where the time of closest approach between the LMC and Leo I satisfied the applied filter of $t_{\min} < -0.5\,\mathrm{Gyr}$.

conserved over the timescale of the encounter.

$$T(t = t_{\min}) + \Phi(t = t_{\min}) = T(t = t_0) + \Phi(t = t_0) \tag{3.2}$$

$$\text{Strong encounter} \Leftrightarrow \Phi(t = t_0) - \Phi(t = t_{\min}) > T(t = t_0) \tag{3.3}$$

$$\text{Strong encounter} \Leftrightarrow \Phi(t = t_0) - \Phi(t = t_{\min}) > T(t = t_{\min}) + \Phi(t = t_{\min}) - \Phi(t = t_0) \tag{3.4}$$

Before the encounter, $\Phi(t = t_0) = 0$. In Sparke and Gallagher (2007) this assumption was made implicitly, by immediately setting the potential difference to $\frac{GM}{r_{\min}}$.

$$\text{Strong encounter} \Leftrightarrow -2\Phi(t = t_{\min}) > T(t = t_{\min}) \tag{3.5}$$

$$\text{Strong encounter} \Leftrightarrow \frac{T(t = t_{\min})}{-\Phi(t = t_{\min})} < 2 \tag{3.6}$$

The distribution of this energy ratio is shown in Figure 3.6. Table 3.1 shows the probabilities of the criterion being satisfied. The probabilities are quite small: only 4.36% for the most favourable scenario (the scenario with the highest probability of an encounter occurring). When only considering realizations where $t_{\min} < -0.5\,\text{Gyr}$, the probability becomes 9.98%. A possible orbit is shown in Figure 3.7. For the same set of initial conditions, the difference between orbits is shown when varying the masses or turning off interactions. The LMC orbit only changes because for a higher M_{LMC}, dynamical friction becomes stronger: notice that for $M_{\text{LMC}} = 5 \times 10^{10}\,\text{M}_\odot$, there is no difference between including or not including interactions.

A simple distance criterion (just selecting orbits where Leo I comes closest to the LMC) gives similar results, but it also selects orbits where LMC and Leo I pass each other at high speed, without much change in the orbit. An example is shown in Figure 3.8.

Criterion		LMC mass ($\text{M}_\odot$)				
	Milky Way	2.5×10^{10}	5×10^{10}	1×10^{11}	1.5×10^{11}	2×10^{11}
$\frac{T(t=t_{\min})}{-\Phi_{LMC}(t=t_{\min})} < 2$	Model 1	66	125	228	329	436
	Model 2	2	4	17	34	55
	Model 3	0	1	4	7	10
$\frac{F_{MW}(t=t_{\min})}{F_{LMC}(t=t_{\min})} < 1$	Model 1	3	22	85	159	230
	Model 2	0	2	6	14	19
	Model 3	0	0	3	7	12

TABLE 3.1: The number of realizations where the two encounter criteria were satisfied (out of the N realizations for which $t_{\min} < -0.5\,\text{Gyr}$, the values of N are listed in Figure 3.3), in the model including inter-satellite interactions and dynamical friction.

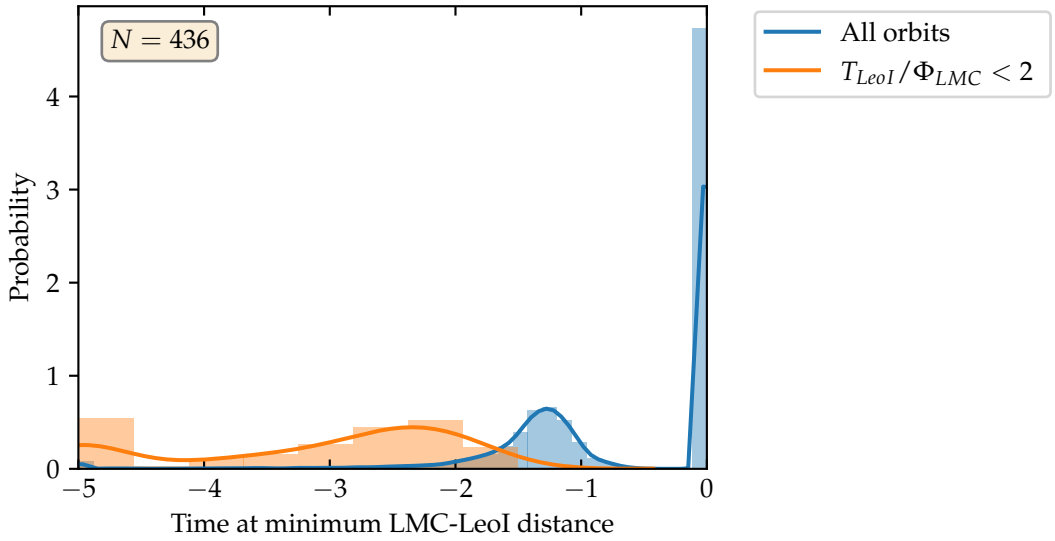

FIGURE 3.4: The distribution of times at minimum Leo I-LMC distance, for the most favourable model (i.e. with the largest probability of an encounter), $M_{\rm LMC} = 2 \times 10^{11}\,{\rm M}_\odot$ and the lightest Milky Way (Model 1, $M_{200} = 9.3 \times 10^{11}\,{\rm M}_\odot$). Firstly, notice that there is a significant fraction of the realizations where this time is at present time. Secondly, notice that the times of minimum distance when the close encounter criterion is satisfied (the orange distribution) is generally much earlier than orbits that do not have an encounter, showing that in these cases, they have been interacting for some time already.

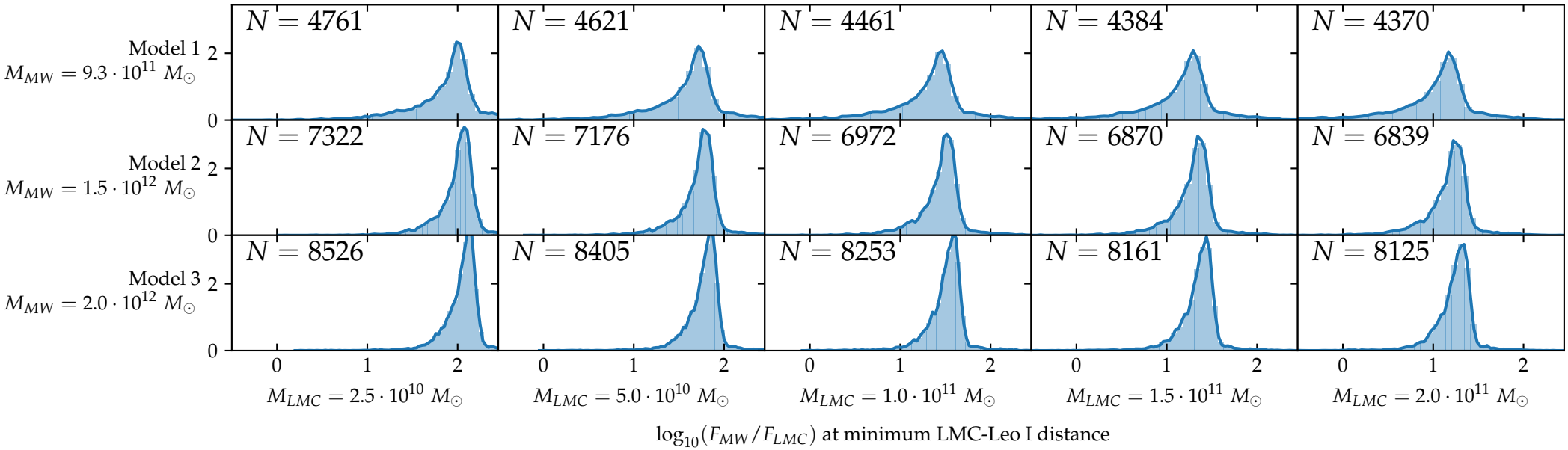

FIGURE 3.5: Force ratio distributions. N indicates the number of realizations where the time of closest approach between the LMC and Leo I satisfied the applied filter of $t_{\min} < -0.5\,\mathrm{Gyr}$.

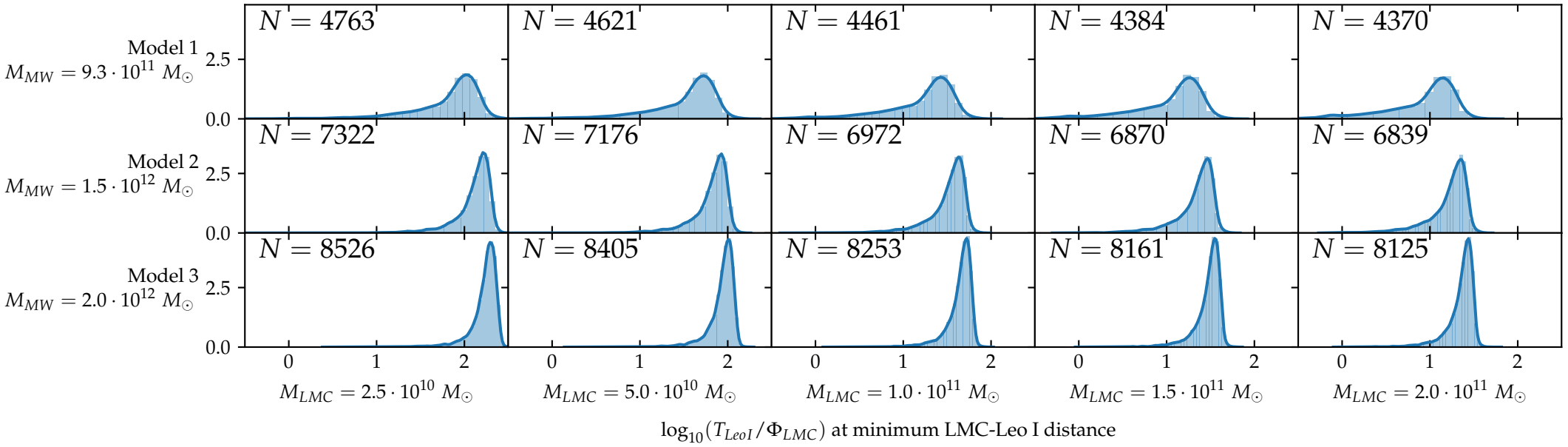

FIGURE 3.6: Distribution of the indicator of the strength of an encounter. N indicates the number of realizations where the time of closest approach between the LMC and Leo I satisfied the applied filter of $t_{\min} < -0.5\,\mathrm{Gyr}$.

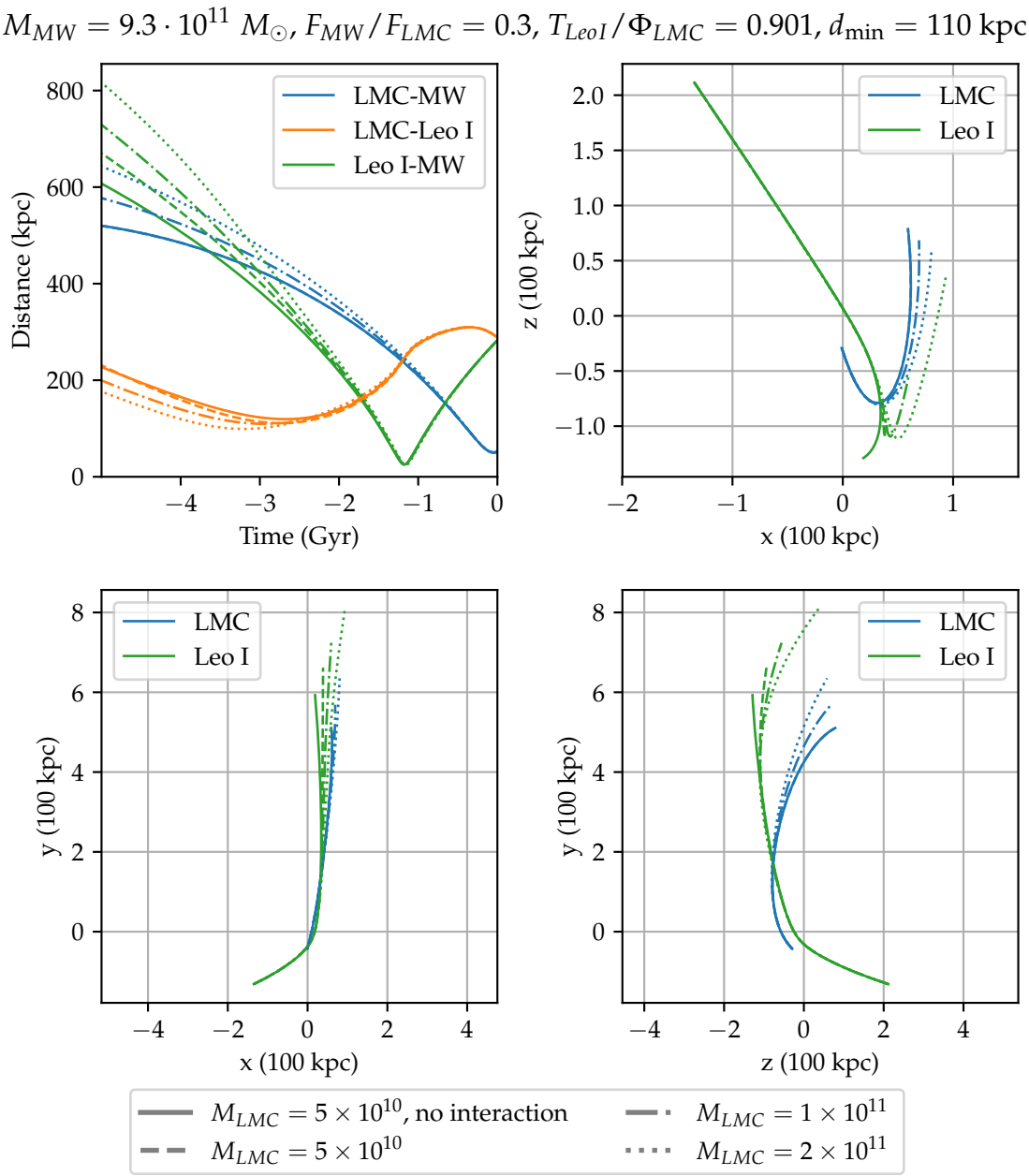

FIGURE 3.7: An example of a case where there is a large change in Leo I's orbit. There is a large difference when comparing the orbits for models that do not include interaction (solid lines) and with interactions included, with different masses (dashed/dotted lines). For example, notice that Leo I is less bound for a massive LMC when looking at their distances at early times ($t = -5$ Gyr). In the orbit plots, one can see a change of the Leo I orbital direction at early times. The numbers in the title refer to a LMC with a mass of $2 \times 10^{11}\ M_\odot$.

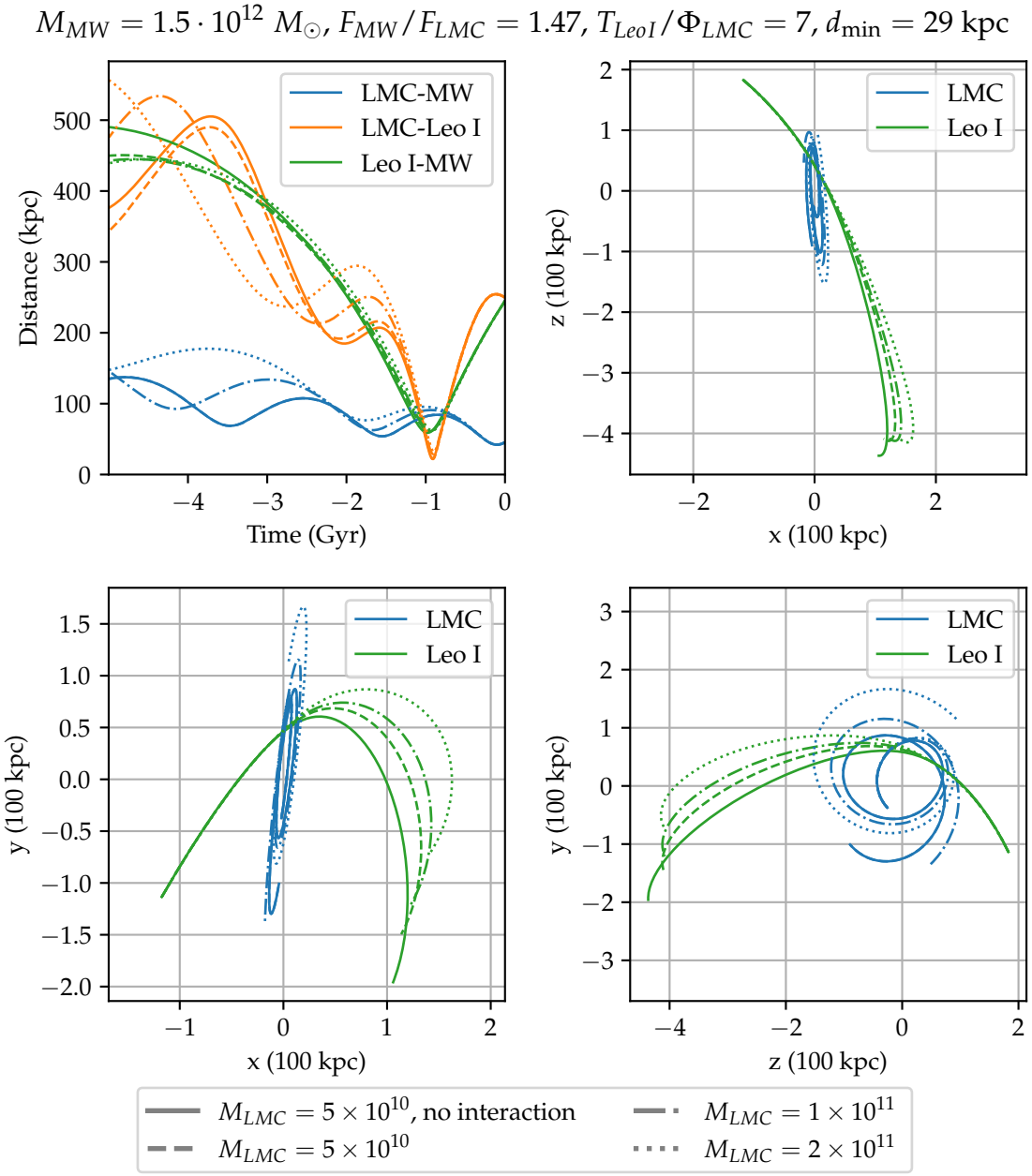

FIGURE 3.8: An example of a case when the LMC and Leo I come very close. In this case, Leo I would have gained energy during its interaction with the LMC. To see that, imagine what would happen to the orbit of Leo I, if it would start at the same distance as the case where interaction was turned on. When integrating forward again, at present time it would end up more bound to the Milky Way. Also, a change in direction of Leo I's orbit occurred, as shown in the orbit plots. The numbers in the title refer to a LMC mass of $2 \times 10^{11}\ M_\odot$.

Chapter 4

Discussion

The question that was asked is whether Leo I could have gained energy by an encounter with the Magellanic Clouds: it does not seem very likely. As shown in Table 3.1, the probabilities of an encounter occurring are small. The most favourable scenario for an encounter taking place combines a low mass Milky Way (of $M_{200} = 9.3 \times 10^{11}\,\mathrm{M}_\odot$) with high mass Magellanic Clouds (of $2 \times 10^{11}\,\mathrm{M}_\odot$). In this case, the probability of the strong encounter criterion being satisfied was 4.36%. If one only considers the realizations in which $t_{\mathrm{min}} < -0.5\,\mathrm{Gyr}$ (i.e. where the LMC and Leo I are not currently at their minimum distance), this probability becomes 9.98%. Lower LMC masses resulted in less realizations where a strong encounter was satisfied. For a heavier Milky Way ($M_{200} = 1.5 \times 10^{12}\,\mathrm{M}_\odot$), the probability was at most 0.55%. In the orbits where a strong encounter did occur, Leo I's orbit changed significantly, both in direction and energy, when comparing the orbits that did and did not consider interactions.

There are many points in this analysis where some not entirely realistic assumptions were made. Here is a summary of the shortcomings and, how it might be possible to improve on them.

First of all, when integrating the orbits I used dynamical friction. This is of itself already an approximation. Much more realistic scenarios could be achieved with N-body simulations, unfortunately these are computationally much more expensive.

Dynamical friction assumes non self-gravitating host particles that interact with the subject body. This is good for an idealized case, but when applying it on extended bodies, some aspects are not as clear. For example, the Coulomb logarithm is assigned in many different ways in literature. Also, hyperbolic paths for the particles were assumed, which is not true for the extended potentials used here. However, these limitations were mitigated reasonably by the choice of a $\ln\Lambda$ that was calibrated to N-body simulations, and even applied to the Magellanic Clouds (Hashimoto, Funato, and Makino, 2003).

Secondly, I modelled the satellites as Plummer spheres. It might be more realistic to use NFW subhalos, maybe including a cut-off to model the effect of tidal stripping, and avoid problems because of its infinite extent.

Another major shortcoming was that all potentials were considered static. The LMC was kept at the same mass, even though tidal stripping would significantly change its mass. Perhaps, it would be nice to include a mass loss model similar to the one proposed in Zentner and Bullock (2003). However, a wide range of LMC masses were considered, so it probably would not change the conclusions.

The LSR velocity I used ($v_{\mathrm{LSR}} = 235\,\mathrm{km/s}$) was also not convolved with any errors in the Monte Carlo analysis. This is not entirely justified, because the norms of the Galactocentric satellite velocities were $(317 \pm 25)\,\mathrm{km/s}$ for the LMC and for Leo I $(236 \pm 51)\,\mathrm{km/s}$, while the uncertainty in v_{LSR} is $\sim$20 km/s. However, convolving v_{LSR} uncertainties might also involve having to change the Galactic potentials. Given

the relatively large differences in the mass distribution at large radii between the different potentials considered, this is likely a minor effect.

Perhaps the largest problem is that the SMC was not taken into account. The reason is that if one simply adds it, for many potentials, it will not stay not bound to the LMC when integrating back. This is a problem with the current setup, which uses a backwards integration scheme. To avoid this problem, it might be better to instead follow the center of mass (CM) of the Magellanic Clouds, calculating the Galactic force on it, and including dynamical friction. Then, after the path of the CM is known, one could calculate the orbits of the LMC and SMC in the CM reference frame. This could avoid the problem of not retaining a bound LMC/SMC, while keeping realistic orbits. An example of an orbit where the LMC and SMC do stay bound when adding them separately, and where there is a large change in Leo I's orbit, is shown in Figure 4.1.

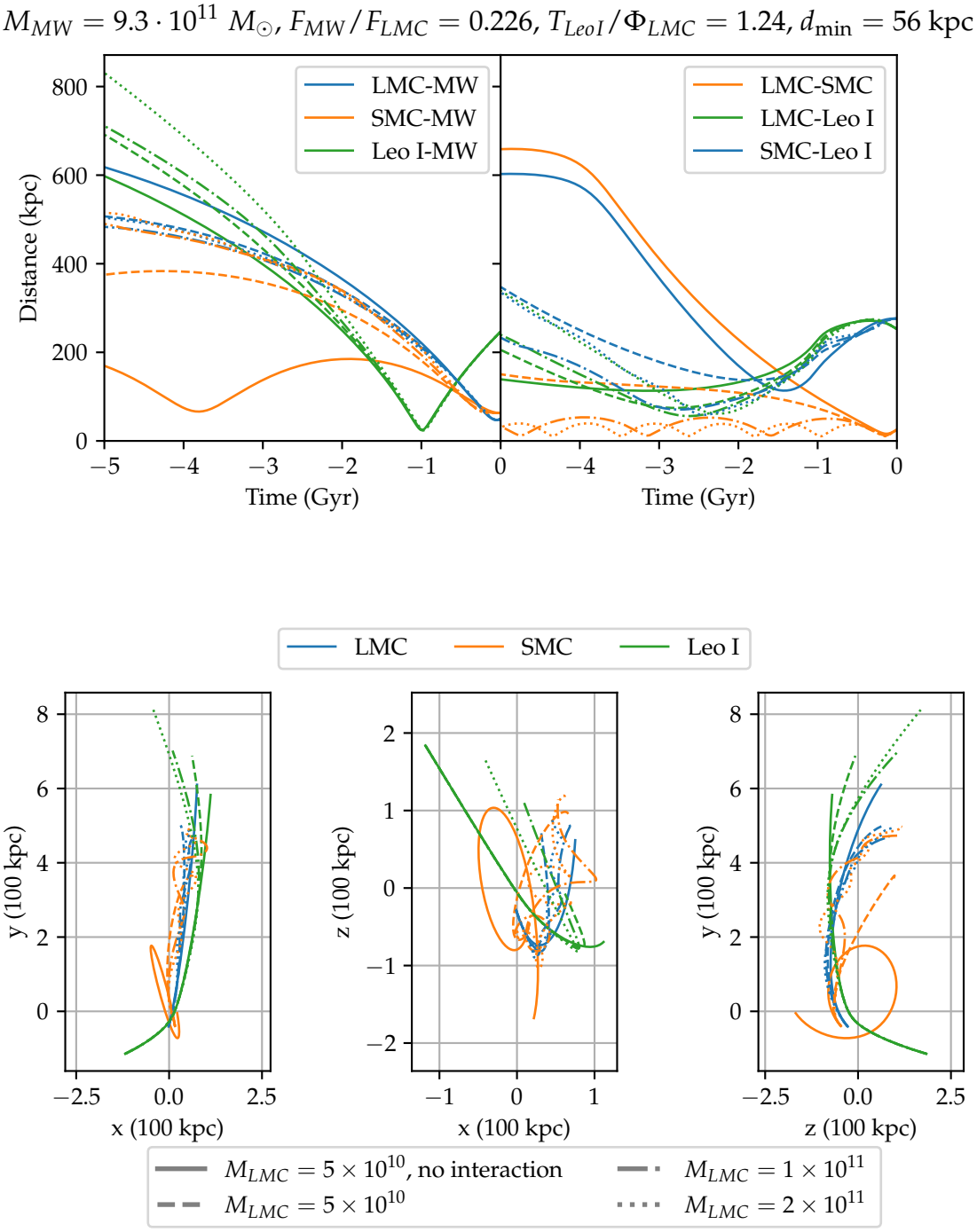

FIGURE 4.1: An example of a realization with an encounter between the Leo I and the Magellanic Clouds, and in which the SMC stays bound to the LMC, especially for the heavy LMC masses.

Bibliography

Astropy developers (2018). *Galactocentric - Astropy v3.0.3*. URL: http://docs.astropy.org/en/stable/api/astropy.coordinates.Galactocentric.html (visited on June 20, 2018).

Bekki, K. (Sept. 2011). "When was the Large Magellanic Cloud accreted on to the Galaxy?" In: MNRAS 416, pp. 2359–2367. DOI: 10.1111/j.1365-2966.2011.19211.x. arXiv: 1106.2379.

Besla, G. (Nov. 2015). "The Orbits and Total Mass of the Magellanic Clouds". In: *ArXiv e-prints*. arXiv: 1511.03346.

Besla, G. et al. (Oct. 2007). "Are the Magellanic Clouds on Their First Passage about the Milky Way?" In: ApJ 668, pp. 949–967. DOI: 10.1086/521385. eprint: astro-ph/0703196.

Binney, J. and S. Tremaine (2008). *Galactic Dynamics: Second Edition*. Princeton University Press.

Bovy, J. (Feb. 2015). "galpy: A python Library for Galactic Dynamics". In: ApJS 216, 29, p. 29. DOI: 10.1088/0067-0049/216/2/29. arXiv: 1412.3451.

Boylan-Kolchin, M. et al. (May 2013). "The Space Motion of Leo I: The Mass of the Milky Way's Dark Matter Halo". In: ApJ 768, 140, p. 140. DOI: 10.1088/0004-637X/768/2/140. arXiv: 1210.6046 [astro-ph.CO].

Buckley, M. R. et al. (May 2015). "Search for gamma-ray emission from dark matter annihilation in the large magellanic cloud with the fermi large area telescope". In: Phys. Rev. D 91.10, 102001, p. 102001. DOI: 10.1103/PhysRevD.91.102001. arXiv: 1502.01020 [astro-ph.HE].

Chandrasekhar, S. (Mar. 1943). "Dynamical Friction. I. General Considerations: the Coefficient of Dynamical Friction." In: ApJ 97, p. 255. DOI: 10.1086/144517.

Correa, C. A. et al. (Sept. 2015). "The accretion history of dark matter haloes - III. A physical model for the concentration-mass relation". In: MNRAS 452, pp. 1217–1232. DOI: 10.1093/mnras/stv1363. arXiv: 1502.00391.

Dutton, A. A. and A. V. Macciò (July 2014). "Cold dark matter haloes in the Planck era: evolution of structural parameters for Einasto and NFW profiles". In: MNRAS 441, pp. 3359–3374. DOI: 10.1093/mnras/stu742. arXiv: 1402.7073.

Gaia Collaboration et al. (Apr. 2018). "Gaia Data Release 2: Kinematics of globular clusters and dwarf galaxies around the Milky Way". In: *ArXiv e-prints*. arXiv: 1804.09381.

Gardiner, L. T. and M. Noguchi (Jan. 1996). "N-body simulations of the Small Magellanic Cloud and the Magellanic Stream". In: MNRAS 278, pp. 191–208. DOI: 10.1093/mnras/278.1.191. eprint: astro-ph/9503095.

Gardiner, L. T., T. Sawa, and M. Fujimoto (Feb. 1994). "Numerical Simulations of the Magellanic System - Part One - Orbits of the Magellanic Clouds and the Global Gas Distribution". In: MNRAS 266, p. 567. DOI: 10.1093/mnras/266.3.567.

Gillessen, S. et al. (Feb. 2009). "Monitoring Stellar Orbits Around the Massive Black Hole in the Galactic Center". In: ApJ 692, pp. 1075–1109. DOI: 10.1088/0004-637X/692/2/1075. arXiv: 0810.4674.

Hashimoto, Y., Y. Funato, and J. Makino (Jan. 2003). "To Circularize or Not To Circularize?-Orbital Evolution of Satellite Galaxies". In: ApJ 582, pp. 196–201. DOI: 10.1086/344260. arXiv: astro-ph/0208452.

Helmi, Amina et al. (2017). "A box full of chocolates: The rich structure of the nearby stellar halo revealed by Gaia and RAVE". In: *Astronomy & Astrophysics* 598, A58.

Kallivayalil, N. et al. (Feb. 2006). "The Proper Motion of the Large Magellanic Cloud Using HST". In: ApJ 638, pp. 772–785. DOI: 10.1086/498972. eprint: astro-ph/0508457.

McConnachie, A. W. (July 2012). "The Observed Properties of Dwarf Galaxies in and around the Local Group". In: AJ 144, 4, p. 4. DOI: 10.1088/0004-6256/144/1/4. arXiv: 1204.1562.

Moster, B. P., T. Naab, and S. D. M. White (Feb. 2013). "Galactic star formation and accretion histories from matching galaxies to dark matter haloes". In: MNRAS 428, pp. 3121–3138. DOI: 10.1093/mnras/sts261. arXiv: 1205.5807.

Murai, T. and M. Fujimoto (1980). "The Magellanic Stream and the Galaxy with a Massive Halo". In: PASJ 32, p. 581.

Navarro, J. F., C. S. Frenk, and S. D. M. White (May 1996). "The Structure of Cold Dark Matter Halos". In: ApJ 462, p. 563. DOI: 10.1086/177173. eprint: astro-ph/9508025.

Planck Collaboration et al. (Sept. 2016). "Planck 2015 results. XIII. Cosmological parameters". In: A&A 594, A13, A13. DOI: 10.1051/0004-6361/201525830. arXiv: 1502.01589.

Price-Whelan, A. M. (Oct. 2017). "Gala: A Python package for galactic dynamics". In: *The Journal of Open Source Software* 2, 388, p. 388. DOI: 10.21105/joss.00388.

Re Fiorentin, P. et al. (Aug. 2005). "Structure in the motions of the fastest halo stars". In: A&A 439, pp. 551–558. DOI: 10.1051/0004-6361:20052911.

Sales, L. V. et al. (Aug. 2007). "Cosmic ménage à trois: the origin of satellite galaxies on extreme orbits". In: MNRAS 379, pp. 1475–1483. DOI: 10.1111/j.1365-2966.2007.12026.x. arXiv: 0704.1773.

Schönrich, R., J. Binney, and W. Dehnen (Apr. 2010). "Local kinematics and the local standard of rest". In: MNRAS 403, pp. 1829–1833. DOI: 10.1111/j.1365-2966.2010.16253.x. arXiv: 0912.3693.

Sohn, S. T. et al. (May 2013). "The Space Motion of Leo I: Hubble Space Telescope Proper Motion and Implied Orbit". In: ApJ 768, 139, p. 139. DOI: 10.1088/0004-637X/768/2/139. arXiv: 1210.6039 [astro-ph.GA].

Sparke, Linda S and John S Gallagher (2007). *Galaxies in the universe: an introduction*. Cambridge University Press.

Weisz, D. R. et al. (May 2013). "Comparing the ancient star formation histories of the Magellanic Clouds". In: MNRAS 431, pp. 364–371. DOI: 10.1093/mnras/stt165. arXiv: 1301.7422.

White, S. D. M. (Feb. 1976). "A note on the minimum impact parameter for dynamical friction involving spherical clusters". In: MNRAS 174, pp. 467–470. DOI: 10.1093/mnras/174.2.467.

Zentner, A. R. and J. S. Bullock (Nov. 2003). "Halo Substructure and the Power Spectrum". In: ApJ 598, pp. 49–72. DOI: 10.1086/378797. arXiv: astro-ph/0304292.

Zhang, X. et al. (Nov. 2012). "Galacto-forensic of Large Magellanic Cloud's Orbital History as a Probe for the Dark Matter Potential in the Outskirts of the Galaxy". In: ApJ 759, 99, p. 99. DOI: 10.1088/0004-637X/759/2/99. arXiv: 1209.3856.